Journal of Molecular Catalysis A: Chemical 291 (2008) 66–74

Contents lists available at ScienceDirect

Journal of Molecular Catalysis A: Chemical

journal homepage: www.elsevier.com/locate/molcata

Low temperature propylene SCR of NO by copper alumina catalyst

Pullur Anil Kumar, Maddigapu Pratap Reddy, Lee Kyung Ju, Bae Hyun-Sook, Ha Heon Phil*

Functional Materials Research Center, Korea Institute of Science and Technology, Cheongryang, Seoul 130-650, Republic of Korea

ARTICLE INFO

Article history:
Received 21 December 2007
Received in revised form 21 April 2008
Accepted 1 May 2008
Available online 18 May 2008

Keywords:
NO reduction to N_2
Copper alumina
Low temperature
Selective catalytic reduction
XPS
In situ DRIFTS

ABSTRACT

NO reduction to N_2 by C_3H_6 was investigated on various copper alumina catalysts prepared by a precipitation method with different copper (Cu) weight percentages to that of aluminium (Al). The catalysts were characterized by X-ray diffraction (XRD), differential thermal analysis (DTA), thermogravimetric analysis (TGA), Fourier transformed infrared (FT-IR) spectroscopy, Brunner Emmett Teller surface area (BET-SA), X-ray photoelectron spectroscopy (XPS), H_2-TPR (temperature programmed reduction) and scanning electron microscopy (SEM) techniques. It is found that the catalyst preparation method as well as the copper content exerts a significant influence on catalytic activity for NO to N_2 conversion. From the DTA analysis it is found that there is a loss of water and CO_2 at 114 to 390 °C and total weight loss by TGA at around 600 °C. A high conversion (70%) of NO to N_2 is obtained by the Cu–Al (3:7) catalyst at 300 °C in the presence of 600 ppm NO_x + 600 ppm C_3H_6 + 8 vol.% O_2. The order of catalysts for higher NO to N_2 conversion is as follows: Cu–Al (3:7) > Cu–Al (2:8) > Cu–Al (4:6) > Cu–Al (1:9) > Cu–Al (7:3). The XPS results show that the Cu–Al (3:7) catalyst calcined at 600 °C possess highly dispersed surface copper (Cu^{2+}) species. The presence of high surface availability of copper (44.8%), in particular as $CuAl_2O_4$ phase, with a high percent intensity of 44 in the Cu–Al (3:7) catalyst is the key to obtaining high efficiency (70%) in a wide range of temperatures (250–400 °C). From in situ diffused reflectance infrared Fourier transformed (DRIFT) spectral analysis, evolution of different intermediate species like $-NO_2$, R–NO, $-COO^-$, –CN, –NCO and $-NH_2$ were observed with varying intensities on different Cu–Al catalysts at different reaction temperatures.

1. Introduction

Nitric oxide (NO) is mainly produced during the combustion of fuels from mobile and stationary sources, such combustion results in serious air pollution by the formation of acid rain, photochemical smog, and green house effect [1]. The reduction of NO can be partially achieved by the modification of combustion devices. However, more effective methods are required for NO reduction to meet the forthcoming strict regulations.

A large number of catalysts have been evaluated in the selective catalytic reduction (SCR) of NO_x by hydrocarbons [2,3]. These catalysts are mainly metal ion-exchanged zeolites (e.g. Cu-, Co-, Fe-, Pt-) and supported platinum group metals (PGMs) such as Pt, Pd, Rh, on various metal oxides (e.g. Al_2O_3, TiO_2, CeO_2) [2–6]. However, the poor stability of metal ion-exchanged zeolites and the deactivation of base metal oxides in the presence of water in the feed constitute the main drawbacks of these catalysts to be used under real lean conditions [2]. Moreover, supported PGMs exhibit rather low selectivity to N_2 and N_2O is formed in substantial amounts [3]. There have been few reports that show the low temperature NO_x reduction activity in the presence of hydrocarbons. In the literature Ag/Al_2O_3 has showed enhanced NO reduction activity in the presence of oxygenated hydrocarbons such as ethanol, acetone, and ether [7–9]. However, there are still two major problems: low-temperature activity and sulfur dioxide poisoning. It is difficult to ensure sufficient catalyst activity to remove NO in the low temperature range of the diesel engine exhaust. Copper catalysts are known to be active at relatively low temperature for the NO reduction in the presence of hydrocarbons.

Transition metal oxides, in particular copper oxides, are known to catalyze many reactions in environmental pollution control, such as CO oxidation and NO reduction by hydrocarbons [10–12]. Catalyst screening studies have shown that supported Cu catalysts exhibit the activity for the SCR, but lack the selectivity for the efficient conversion of NO to N_2 in a wide temperature range [13–15]. A critical issue that needs to be addressed is the control of catalyst activity and selectivity. That is why it is of interest to study the nature and reactivity of nitrogen oxides on the surface of copper alumina with hydrocarbons [16–18].

* Corresponding author. Tel.: +82 2 958 5461; fax: +82 2 958 5379.
E-mail addresses: pulluranil@yahoo.co.in (P.A. Kumar), pratapiict@yahoo.co.in (M.P. Reddy), heonphil@kist.re.kr (H.H. Phil).

1381-1169/$ – see front matter © 2008 Elsevier B.V. All rights reserved.
doi:10.1016/j.molcata.2008.05.006

Copper-containing hydrotalcites (HT) represent a rather peculiar system in this family of compounds, probably due to the well-known tendency of copper to form distorted octahedra because of the Jahn–Teller effect in the presence of a large excess of M(II) over the M(III) cations in the HT structure [19]. Much effort has been made to prepare hydrotalcites containing copper, to be used for different purposes. For example copper hydrotalcites with carbonate as the interlayer anion have been used by Corma et al. [20] as catalyst precursors for the catalytic removal of SO_x and NO_x. The catalytic production of hydrogen by steam reforming of methanol has been carried out over several Cu-containing layered double hydroxides (LDH) [21]. Cu–Al or Cu–M^{2+}–Al hydrotalcites have also been tested as catalyst precursors in the liquid-phase hydrogenation of cinnamaldehyde [22]. The Cu–Al_2O_3 catalyst prepared by adsorption of Cu^{2+} from a basic solution showed a higher activity than the one prepared by the conventional impregnation method. This is because the basic solution preparation is favourable to the formation of isolated CuO-like species, which are believed to be the active sites for NO reduction [23]. Apparently, the preparation method seems to be a critical factor for the activity of Cu–Al_2O_3 catalyst for NO reduction by hydrocarbons.

In order to achieve higher NO to N_2 conversions in a wide temperature range, the copper alumina catalysts were prepared by a co-precipitation method and their efficiency for deNO_x was tested. Activity measurements were carried out using a reaction mixture of 600 ppm NO, 600 ppm C_3H_6, and 8 vol.% O_2. LDH structure and Cu^{2+} phase in the form of cuprous oxide (CuO) and copper aluminate ($CuAl_2O_4$) phases were scrutinized to check relations between structure and catalytic efficiency. Prepared catalysts were characterized in detail for the state of dispersed copper ions and active phases (CuO and $CuAl_2O_4$) by XRD, FT-IR, TPR and XPS analysis. The reaction was also studied by in situ DRIFT (diffused reflectance infrared Fourier transformed) spectroscopy for analyzing the dynamic mechanistic measurements of the complex interplay between formation and desorption/oxidation of NO (adsorbed) and partial oxidation species of the propylene. The intensities of various intermediates formed during the reaction were analyzed and discussed by in situ DRIFT spectroscopy study.

2. Experimental

2.1. Preparation

Copper alumina catalysts were prepared with different Cu^{2+}/Al^{3+} atomic ratios by a co-precipitation method. A basic solution was prepared from 2 M NaOH and 1 M Na_2CO_3 (S_1) and an aqueous solution of Cu(II) and Al(III) nitrates (S_2) was prepared with different Cu^{2+}/Al^{3+} atomic ratios (1:9, 2:8, 3:7, 4:6 and 7:3). They were taken into two separating funnels. The solutions S_1 and S_2 were added dropwise to a beaker containing 1000 mL of distilled water under vigorous stirring. The addition of both solutions is controlled by monitoring pH regulation (8.0–8.5) with a pH electrode immersed in the solution. The resulting solution was aged for an hour at 60–70 °C with vigorous stirring. It then followed several washings with distilled water to attain neutral pH. Then the solution was filtered and the resulting precipitate was oven dried for 12 h, and subsequently calcined at 600 °C for 5 h in static air.

2.2. Characterization

X-ray diffraction (XRD) patterns were recorded using a Bruker D8 Advance with Cu Kα radiation and operated at 40 kV and 20 mA. The fine powders were scanned (2θ) in the range from 10 to 80. BET surface area was obtained from N_2 adsorption isotherms measured at −196 °C using a Micromeritics Autochem II-2720 instrument. The DTA/TGA (differential thermal analysis/thermogravimetric analysis) experiments were performed with a NETZSCH TG/DTA 209 instrument. Fifty milligrams of the sample were placed in a microbalance crucible and heated in a flow of Ar (50 cm^3/min) up to 800 °C at 10 °C/min and a final hold-up of 20 min. Temperature programmed reduction (TPR) experiments were carried out on a Micromeritics Autochem II-2720 chemisorptions instrument using 5% H_2/Ar gas at a flow rate of 30 cm^3/min. 50 mg of sample was taken in a U-shaped quartz cell and heated under the flow of 5% H_2/Ar at a temperature ramp speed of 5 °C/min from room temperature to 600 °C. Calibration was made by reduction of a known amount of pure standard cupric oxide powder under similar experimental conditions. Fourier transform infrared spectra (FT-IR) were obtained in the range of 4000–400 cm^{-1} by diluting the samples (1%) with KBr powder and measured on a JASCO FT/IR-4200 Fourier transform infrared spectrometer. The X-ray photoelectron spectra (XPS) were collected with a PHI 5800 ESCA system. Al Kα ($h\nu$ = 1486.6 eV) was used as X-ray source. The elemental analysis (ICP technique) is done using the PerkinElmer ELAN DRC plus system. Prior to the ICP analysis, samples were dissolved in acidic solution of HNO_3 + HCl + H_2SO_4 + distilled water and vaporized by heating. Scanning electron microscopy (SEM) pictures were taken by Hitachi S-4200 FE-SEM at an acceleration voltage of 15 kV.

2.3. Activity measurements

NO reduction with propylene (C_3H_6) in the presence of an excess amount of O_2 was performed with a fixed-bed flow-type quartz reactor. Prior to the reaction, the catalyst (usually 0.3 g) was pretreated with 10% O_2/He flow at 500 °C for 1 h. The feed mixture consisted of 600 ppm NO, 600 ppm C_3H_6, and 8 vol.% O_2 balance helium; 0.3 g of catalyst was used at a total flow rate of the reaction gas mixture, 120 cm^3/min. The NO concentrations were analyzed with an online NDIR Fuji NO analyzer. Other reactants and products were analyzed online by using a Varian Micro GC equipped with a TCD. The concentrations of C_3H_6, CO_2 and N_2O were detected by a Parapak Q column. A molecular sieve 5A column was used to monitor the formation of CO and N_2. All the catalysts were tested and the conversions of NO to N_2, NO to N_2O and C_3H_6 to CO_x were calculated by using the formula as follows:

- Conversion of NO to N_2 = 2 $[N_2]/NO^{in} \times 100$.
- Conversion of NO to N_2O = 2 $[N_2O]/NO^{in} \times 100$.
- Conversion of C_3H_6 to CO_x = $(C_3H_6{}^{in} - C_3H_6{}^{out})/C_3H_6{}^{in} \times 100$.
- NO^{in} = initial amount of NO.
- $C_3H_6{}^{in}$ = initial amount of C_3H_6.
- $C_3H_6{}^{out}$ = amount of C_3H_6 left after reaction.

2.4. In situ DRIFTS measurements

In situ DRIFT spectroscopy measurements were performed on a JASCO FT/IR-4200 Fourier transform infrared spectrometer, equipped with an in situ diffuse reflection chamber and a high sensitivity MCT/A detector cooled by liquid nitrogen. DRIFT spectra were recorded at 4 cm^{-1} resolution as an average of 50 scans using the MCT/A detector. Finely grind powdered catalyst was taken in an alumina crucible, and placed in a DRIFTS cell. The spectra were measured to monitor the in situ NO reduction mechanism for the catalysts at different temperatures within the range of 175–350 °C. The DRIFTS cell is fitted with BaF_2 windows. Prior to each experiment 0.03 g of catalyst was heated at a rate of 10 °C/min from room temperature to 500 °C under helium flow. After a period of 30 min stay the sample was cooled down to 175 °C in helium flow. After pretreatment the background spectrum under helium flow was

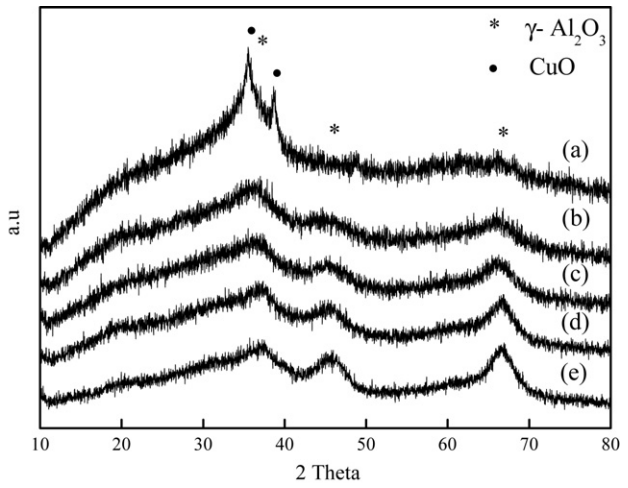

Fig. 1. XRD patterns of the calcined catalysts (a) Cu–Al (7:3); (b) Cu–Al (4:6); (c) Cu–Al (3:7); (d) Cu–Al (2:8); (e) Cu–Al (1:9).

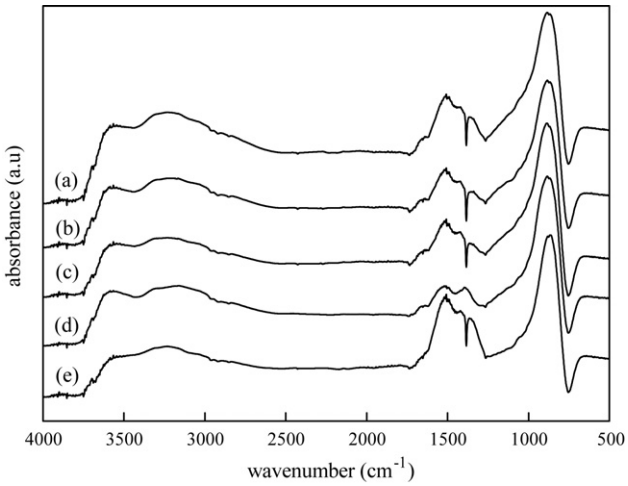

Fig. 3. FT-IR spectra of calcined catalysts (a) Cu–Al (4:6); (b) Cu–Al (3:7); (c) Cu–Al (2:8); (d) Cu–Al (1:9); (e) Cu–Al (7:3).

collected at 175 °C. The reaction gas mixture consisting of 600 ppm NO, 600 ppm C_3H_6, 8 vol.% O_2 and balance helium was fed at a flow rate of 100 cm^3/min on to the catalyst at desired temperatures. A reference spectrum of the catalyst in helium flow was subtracted from each spectrum taken under a flow of reaction mixture gas.

3. Results and discussion

3.1. XRD

The XRD patterns of the calcined Cu–Al catalysts are shown in Fig. 1. All the calcined catalysts show highly amorphous nature with low intensity broad peaks. The calcined sample shows diffraction lines that can be assigned to γ-Al_2O_3 (JCPDS file no. 10-0425). Only the catalyst containing higher percentage of copper, Cu–Al (7:3), shows the diffraction lines that can be assigned to the CuO phase (JCPDS file no. 65-2309).

3.2. FT-IR

The FT-IR spectra of the oven dried samples containing LDHs (layered double hydroxides) (Fig. 2) resemble those of hydrotalcite like phases [24]. Typical of these spectra are the strong broad absorbance band between 3600 and 3200 cm^{-1} associated with the stretching mode of hydrogen-bonded hydroxyl groups from both the hydroxide layers and interlayer water. This broad band intensity of oven-dried samples increased with the increase in weight percentage of copper from Cu–Al (1:9) to Cu–Al (7:3) corresponding to the increase in hydroxyl groups in both the hydroxide layers and interlayer water. A bending vibration band corresponding to a water deformation δ(H_2O) is seen at 1635 cm^{-1}. In most of the samples, there are two IR active absorption bands arising from the carbonate anions observed at 1500–1350 cm^{-1} (ν_3) and 1070–810 cm^{-1} (ν_2). However, all samples show two bands in the region 1500–1350 cm^{-1}, which may be attributed either to the disordered nature of the interlayer or to a lowering of the symmetry of the carbonate anions from D_{3h} to C_{2V} in the interlayer, which lifts the degeneracy of the ν_3 mode [24]. Observation of the ν_1 mode around 1030 cm^{-1} also suggests a lowering of the symmetry of the carbonate ion. The presence of carbonate ions is also observed and the intensity increased with percentage of copper, but more hydroxyls are found compared to carbonate species with respect to intensity.

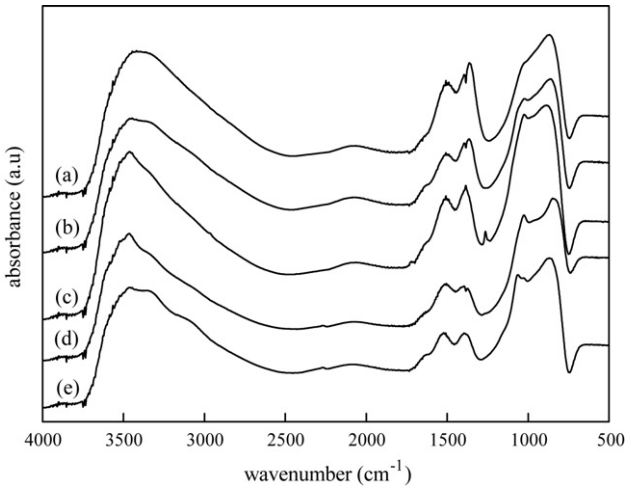

Fig. 2. FT-IR spectra of oven-dried catalysts (a) Cu–Al (7:3); (b) Cu–Al (4:6); (c) Cu–Al (3:7); (d) Cu–Al (2:8); (e) Cu–Al (1:9).

The FT-IR spectra of the calcined Cu–Al samples are shown in Fig. 3. A common band at 3600–3200 cm^{-1} is observed, which may be assigned to the stretching mode of the remaining hydrogen-bonded hydroxyl groups in the calcined catalysts. A comparison between the FT-IR spectra of the calcined and oven-dried samples shows that the intensity of the hydroxyl groups of calcined samples is drastically decreased due to the removal of physisorbed and interlayer water and the dehydroxylation of the lattice water at higher temperatures. Observation of the ν_1 mode around 1050 cm^{-1} also suggests a lowering of the symmetry of the carbonate ion. Significant changes are observed in the low frequency region associated with changes in lattice structure, and the intensity of the cation–oxygen vibrational bands is significantly increased in calcined catalysts compared with the oven dried ones. As expected, IR absorption bands arising from the carbonate anion of the oven dried catalysts are decreased in intensity because of decomposition of the interlayer anion in calcined samples.

3.3. DT/TGA

The TGA/DTA patterns (Fig. 4) for the oven dried catalyst Cu–Al (3:7) indicate general loss from low temperatures to high temperatures due to the loss of water and CO_2. The low temperature loss

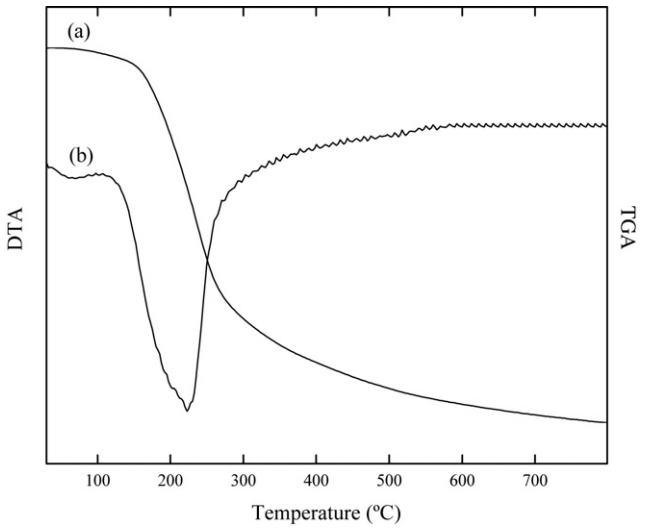

Fig. 4. (a) TGA and (b) DTA plots for the Cu–Al (3:7) oven-dried catalyst.

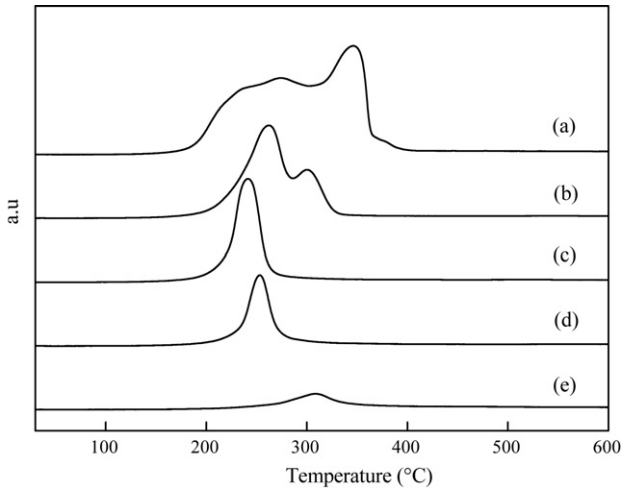

Fig. 5. TPR patterns of the catalysts (a) Cu–Al (7:3); (b) Cu–Al (4:6); (c) Cu–Al (3:7); (d) Cu–Al (2:8); (e) Cu–Al (1:9).

corresponding to the reversible removal of physisorbed and interlayer water (from both the internal and external surfaces) without collapse of the structure extends from approximately 100 to 200 °C. At higher temperatures in the range of 200–320 °C the loss arises from the dehydroxylation of the lattice as well as decomposition of the interlayer carbonate anions [24]. It is clearly seen from XRD of calcined samples that the layered structure is destroyed since no characteristic reflections of LDHs are present in the XRD patterns, but some broad diffraction peaks that are obviously different from that of single metal oxide phases such as alumina and copper oxide are detectable in the amorphous nature of XRD pattern. All the prepared catalysts show high surface areas, which are shown in Table 1. The surface areas of the catalysts are decreased with gradual increase in copper weight percentage. The high surface area of the catalysts is well correlated with observed amorphous nature of the catalysts (after calcination) in X-ray diffractograms (Fig. 1). The weight percentages of copper present in the catalysts were analyzed from the ICP analysis and are given in Table 1.

3.4. TPR

In order to elucidate the nature of the copper species present in the prepared catalysts, the TPR experiment was performed. The TPR profiles are shown in Fig. 5 and the amount of hydrogen consumption of the Cu–Al catalysts is summarized in Table 2. The molar ratio of hydrogen consumption to the amount of copper indicates the degree of reduction. The reduction behavior of Cu–Al catalysts is characterized by the fact that the loading of copper increases the number of reduction peaks. The lower loadings of copper catalysts show a single reduction peak up to Cu–Al (3:7) and a further increase in copper weight percentage is associated with the appearance of more than one reduction peak. In the Cu–Al (1:9) catalyst a single reduction peak is observed at T_{max} of 309 °C. When the copper loading increases from Cu–Al (1:9) to Cu–Al (3:7), the T_{max} of the single reduction peak decreases to lower temperatures and the amount of hydrogen consumption also increases. Fernández-García et al. [23] observed that the single low temperature reduction peak at lower loadings corresponds to the reduction of Cu^{2+} in the surface $CuAl_2O_4$. This low temperature peak may also be due to the reduction of amorphous, highly dispersed bulk-like CuO phase [25], which could not be detected by XRD (Fig. 1). The higher loadings of Cu–Al (4:6) and Cu–Al (7:3) show more than one reduction peak at T_{max} of 262, 300 and 230, 346 °C. These peaks at higher loadings of Cu–Al catalysts are divided into low temperature reduction peaks, which may correspond to the reduction of Cu^{2+} to Cu^{+}, and a high temperature peak for the reduction of Cu^{+} to Cu^{0}. In contrast, at lower loadings the single reduction peak corresponds to the direct reduction of Cu^{2+} to Cu^{0} [26]. For the quantitative analysis,

Table 2
H_2-TPR results of all fresh catalysts

Catalyst	T_{max} (°C)	H_2 consumption (μmol/g)		
		Cu^{2+}	Cu^{+}	Total
Cu–Al (1:9)	309	28.9	–	28.9
Cu–Al (2:8)	253	66.5	–	66.5
Cu–Al (3:7)	241	100.3	–	100.3
Cu–Al (4:6)	262	95.7	–	153.1
	300	–	57.4	–
Cu–Al (7:3)	230	150.2	–	255.3
	346	–	105.1	–

Table 1
BET-surface area, ICP and XPS analysis results of all catalysts

Catalyst	BET-SA (m^2/g)	% NO to N_2 at 300 °C	wt% of Cu		% of copper (surface to bulk ratio)	% Intensity of Cu (2p) XPS analysis		
			ICP (bulk)	XPS (surface)		Cu^{2+} in $CuAl_2O_4$ (935.0 eV)[a]	Cu^{2+} in CuO (933.8 eV)[a]	Cu^{+} in Cu_2O (932.7 eV)[a]
Cu–Al (1:9)	355	43	4.67	1.09	23.3	12	77	11
Cu–Al (2:8)	350	61	8.9	3.07	34.4	30	62	8
Cu–Al (3:7)	335	70	13.7	6.15	44.8	44	54	2
Cu–Al (4:6)	320	55	19.9	6.93	34.8	30	46	24
Cu–Al (7:3)	295	30	41.7	11.17	26.7	2	19	79

[a] Binding energy.

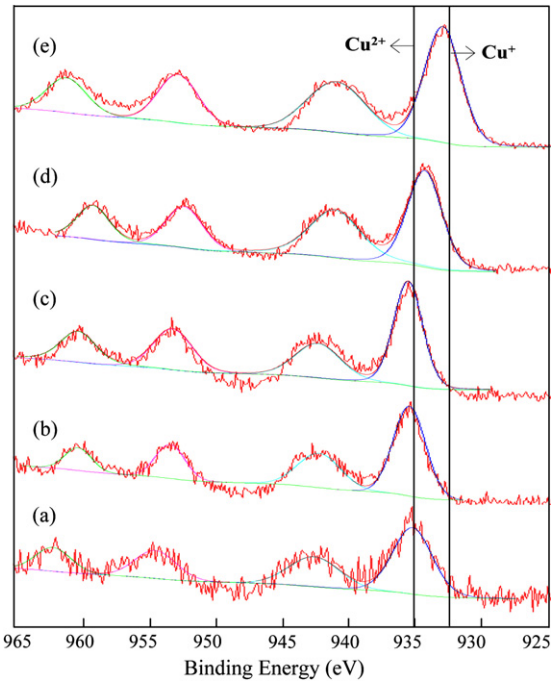

Fig. 6. XPS spectra of the catalysts (a) Cu–Al (1:9); (b) Cu–Al (2:8); (c) Cu–Al (3:7); (d) Cu–Al (4:6); (e) Cu–Al (7:3).

all of the peaks that can be differentiated by the computer software have been integrated to evaluate their individual amounts. Table 2 represents the amount of hydrogen consumptions of the two copper species (Cu^{2+} and Cu^{+}) present in Cu–Al catalysts of different loadings. Even though the Cu–Al catalysts of higher loadings show higher hydrogen consumption than Cu–Al (3:7), the peak corresponding to Cu^{2+} is prevalent (almost 100%) in Cu–Al (3:7). Hence the Cu–Al (3:7) catalyst attains the highest conversion rates at lower temperatures. The amount of hydrogen consumption (Table 2) over the Cu–Al (7:3) catalyst is 255.3 μmol/g, and lower H_2 uptakes are observed with the catalysts of low copper loadings.

3.5. XPS

The Cu 2p photoelectron spectra of the different catalysts, obtained by XPS analysis are shown in Fig. 6. From the figure it is clearly observed that with increasing weight percent of Cu the binding energy (B.E) of the Cu 2p shifted towards lower energy. From Fig. 6 it is observed that the catalysts of higher copper loadings show a maximum percent intensity of the Cu 2p peak at a binding energy of 932.7 eV, which is due to the Cu_2O phase. With decreasing Cu weight percentage the percent intensity of the Cu 2p peak shifts towards higher binding energies, which are observed at 933.8 and 935.0 eV and are due to CuO and $CuAl_2O_4$, respectively [27]. The percent intensities of different copper phases Cu_2O (932.7 eV), CuO (933.8 eV) and $CuAl_2O_4$ (935.0 eV) [27] present over different catalysts are given in Table 1. With increasing copper loading to Cu–Al (3:7), the total percent intensity of Cu 2p (933.8, 935.0 eV) due to Cu^{2+} phases (CuO, $CuAl_2O_4$) increases and then decreases to a least percent intensity of 21 for Cu–Al (7:3). Correspondingly the percent intensity of Cu 2p (932.7 eV) due to the Cu^{+} phases (Cu_2O) decreased and then increased to a maximum of 79 for the Cu–Al (7:3) catalyst. From this observation it may be concluded that the Cu–Al (3:7) catalyst has highest percentage of active Cu^{2+} phases which will contribute to high catalytic activity for the conversion of NO to N_2 [28]. In the case of catalysts of higher copper loadings photoelectron lines due to CuO, $CuAl_2O_4$ and Cu_2O are observed. At lower loadings of Cu–Al catalysts, Cu–Al (3:7) has the Cu $2p_{3/2}$ binding energy of 935.2 eV, which is similar to that of Cu^{2+} and the same as that of $CuAl_2O_4$, in good agreement with the literature [29–31]. The presence of Cu^{+} oxidation state at higher loadings is in good agreement with the TPR results which show an additional high temperature reduction peak corresponding to Cu^{+} in Cu_2O. When the loading of copper is increased beyond a certain extent (Cu–Al (3:7)), the $CuAl_2O_4$ phase disappears from the surface and CuO/Cu_2O phases prevail. Shimizu et al. [17] mentioned that the presence of a high percentage of the $CuAl_2O_4$ (935.0 eV) phase leads to high catalytic activity. This is also well correlated with our observation by XPS analysis (Table 1) that the percent intensity of photoelectron lines (935.0 eV) of the $CuAl_2O_4$ phase increases with an increase in Cu loading to a maximum of 44% for Cu–Al (3:7) and then decreases further by an increase in the Cu loading. From the ICP and XPS analyses we also deduce the amount of total copper available on the surface of the catalysts by calculating the surface to bulk ratio. The surface availability of copper is increased with increasing weight percentage of copper to a maximum of 44.8% for Cu–Al (3:7) and then decreased. These values also well support and prove that the catalyst loaded with a copper content of 30% has highly active phases and shows high conversion of NO to N_2 in a wide range of temperatures, which is further discussed and correlated in Section 3.6.

3.6. NO conversion

Preparation method, copper loading and calcination temperature are generally considered to be important factors for the structure and dispersion of copper alumina catalysts, and they commonly influence the catalytic performance of the catalysts. In literature it is well reported that the calcination temperatures could not influence much the NO conversion to N_2 but influence the formation of the $CuAl_2O_4$ phase in catalysts [32]. As a consequence, in this investigation calcined all the prepared catalysts were calcined at a maximum temperature of 600 °C to attain high surface availability of the $CuAl_2O_4$ phase. The calcined catalysts were amorphous which is shown in XRD patterns of the catalysts having high surface area with decreasing 'Cu' weight percentage (Table 1). It is also observed that with increasing the Cu weight percentage, the conversions of NO to N_2 are increased up to a maximum efficiency of 70% at 300 °C for Cu–Al (3:7) (Table 1). With further increase in Cu loading, the conversion of NO to N_2 is decreased. This may be due to the agglomeration of Cu nanoparticles with an increase in the Cu content, (Fig. 7) which leads to the decrease in the surface area and a lesser surface availability of the active phases (Table 1).

Fig. 8 shows the conversions of NO to N_2 over the Cu–Al catalysts with varying Cu/Al ratio. The optimal concentration of the copper loading on the impregnated catalysts is well established in the literature [28], but there are not many reports on the precipitated catalysts, particularly for $DeNO_x$ reaction. An exception is the finding of Chen et al. [33], who reported lower conversions of NO to N_2. In the present study we are able to achieve a considerable maximum efficiency of 70% conversion of NO to N_2 with 30 wt% of Cu loading at a lower temperature of 300 °C and also attain considerably high conversions in a wide temperature range of 250–400 °C. The catalytic activity of NO conversion to N_2 with propylene as reducing agent on the series of Cu–Al catalysts is significantly affected by the copper loading. With increasing copper content from 10 to 30% in Cu–Al catalysts, maximum NO reduction to N_2 increases and then decreases. In the Cu–Al (4:6) catalyst the maximum conversion of NO to N_2 is observed at a lower temperature of about 250 °C, but the activity decreases at higher temperatures, which is also in agreement with the literature that higher loadings of copper cata-

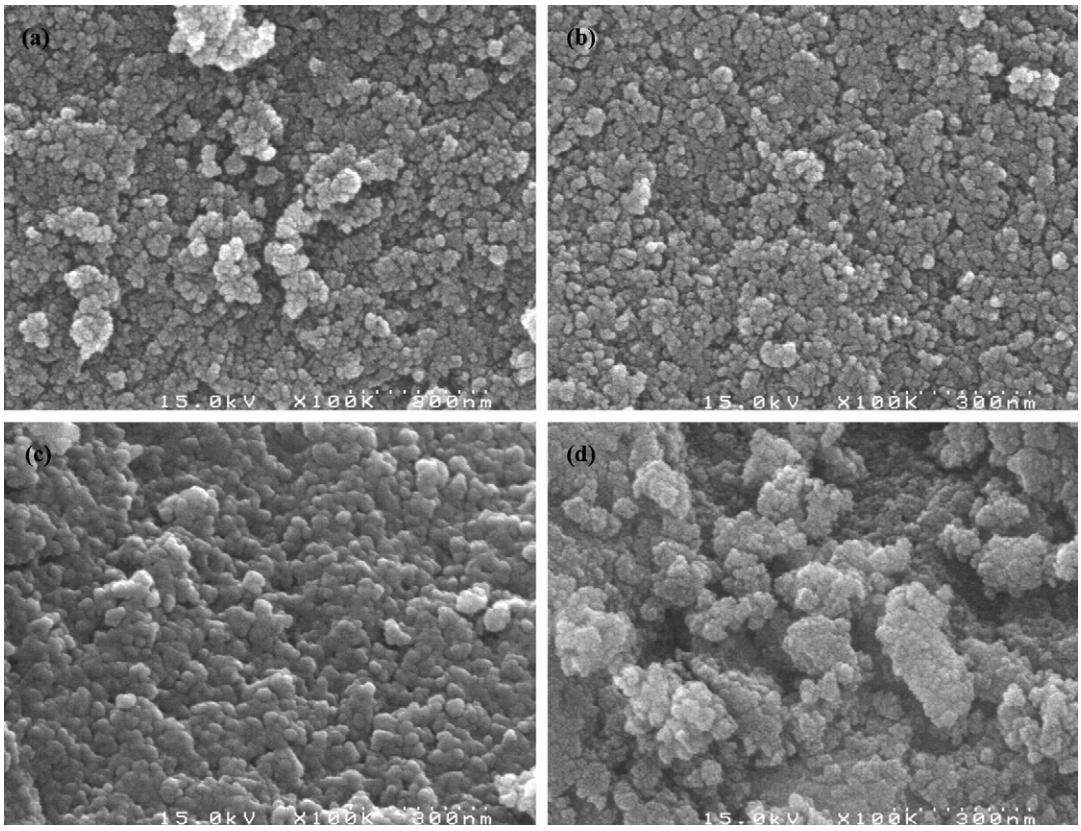

Fig. 7. SEM images of the catalysts (a) Cu–Al (1:9); (b) Cu–Al (3:7); (c) Cu–Al (4:6); (d) Cu–Al (7:3).

lysts enhance low temperature activity [33]. The high performance at lower temperatures of the studied catalysts seems to be due to the high dispersion of copper particles and small size of deposited copper species on alumina (Fig. 7), formed during the precipitation using a combination of both Na_2CO_3 and NaOH solutions. The data of XPS analysis (Table 1) show that the Cu–Al (3:7) catalyst possesses a highly dispersed surface with high percent intensity of $CuAl_2O_4$ phases. Therefore, the $CuAl_2O_4$ is believed to be a more active phase for NO reduction to N_2 by propylene than the highly dispersed surface and bulk CuO. The widest temperature range activity was observed over the Cu–Al (3:7) catalyst with higher than 45% of NO conversion to N_2 in the temperature ranging from 250 to 400 °C. Fig. 9 shows the conversion of propylene to CO_x on various Cu–Al catalysts. The total conversion of propylene is observed at 300 °C over all the catalysts. The Cu–Al (4:6) catalyst displays higher conversion of about 85% at 275 °C than the other catalysts, and it is also shown the highest NO to N_2 conversion at this temperature. The NO to N_2O conversion is observed to be less than 5% over all the catalysts studied (Fig. 8).

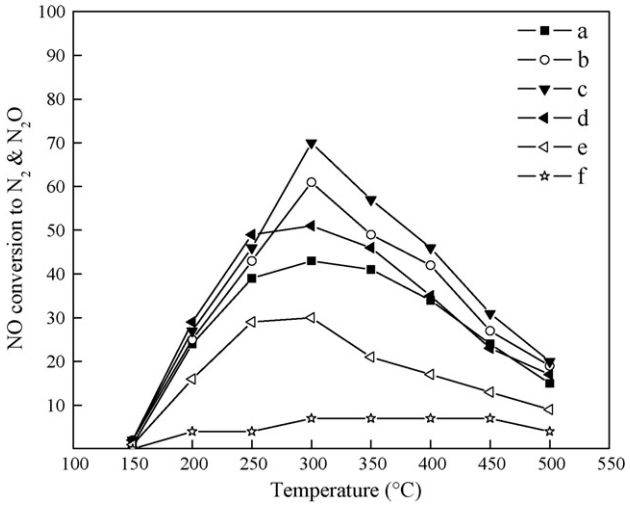

Fig. 8. Conversion of NO to N_2 of the catalysts (a) Cu–Al (1:9); (b) Cu–Al (2:8); (c) Cu–Al (3:7); (d) Cu–Al (4:6); (e) Cu–Al (7:3); (f) NO to N_2O of Cu–Al (3:7). Conditions: 600 ppm NO, 600 ppm C_3H_6, 8 vol.% O_2, balance helium; 0.3 g of catalyst; total flow rate—120 cm^3/min.

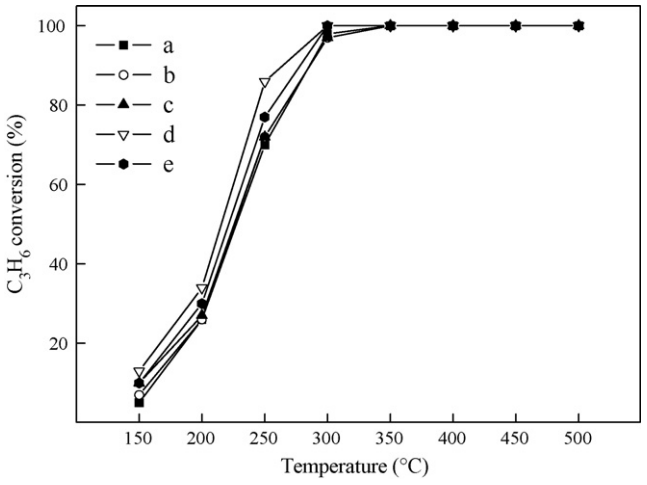

Fig. 9. Propylene conversion of the catalysts (a) Cu–Al (1:9); (b) Cu–Al (2:8); (c) Cu–Al (3:7); (d) Cu–Al (4:6); (e) Cu–Al (7:3). Conditions: 600 ppm NO, 600 ppm C_3H_6, 8 vol.% O_2, balance helium; 0.3 g of catalyst; total flow rate—120 cm^3/min.

3.7. In situ DRIFTS studies on nitric oxide reduction

In situ DRIFTS on the different catalysts are investigated as an attempt to see whether the differences in the activities are reflected in the fundamental bands observed from the DRIFT spectra. The DRIFT spectra were recorded during $NO + C_3H_6 + O_2$ reaction in the steady state on various catalysts at 275 °C. Fig. 10(i), (ii) and (iii) shows the DRIFT spectra of various catalysts at 275 °C in a flow of mixture gas containing $NO + C_3H_6 + O_2$. The catalysts show two main bands due to acetate at 1590–1580 and 1454 cm^{-1}, together with bands due to carbonyl (1729 cm^{-1}), carbonate species (1643, 1312, and 1277 cm^{-1}), formate (1377 cm^{-1}), Al–NCO (2234 cm^{-1}), Cu–NCO (2197 cm^{-1}), and CN species (2150 cm^{-1}) [17]. These results indicate that the acetate is the main adsorbed species during the reaction on the series of catalysts tested. The weak band observed at 1303 cm^{-1} is assigned to unidentate nitrate, and the 1277, 1312, and 1551 cm^{-1} bands are assigned to bidentate nitrate species. With increasing weight percentage of copper from 10 to 40%, the intensities of the 1643 and 1454 cm^{-1} bands increase and subsequently decrease. The Cu–Al (1:9) catalyst shows a high intensity peak of Al–NCO, and with further increasing copper content the peak corresponding to the Cu–NCO intensity increases with the gradual decrease in the Al–NCO peak intensity. However, the intensity of Al–NCO is very low and the intensity of Cu–NCO is significantly high in Cu–Al (3:7) catalyst. Note that the Cu–Al (3:7) catalyst shows wide temperature range activity and high selectivity particularly at low temperatures. In the O–H stretching region of the spectra the band with negative absorbance that appeared at 3770 cm^{-1} also decreases with copper loading.

The DRIFT spectra were recorded on the Cu–Al (3:7) catalyst (Fig. 11(i), (ii) and (iii)) during the exposure to the mixture gas containing $NO + C_3H_6 + O_2$ for 100 min at different temperatures from 175 to 350 °C under steady state conditions. Shimizu et al. [34] reported several distinct IR bands observed at 1303, 1312 and 1551 cm^{-1}, which are assigned to unidentate nitrate (1303 cm^{-1}), and bidentate one (1312 and 1551 cm^{-1}) [35,36]. He et al. [37] observed that the intensities of the bands at 1312 and 1551 cm^{-1} assigned to nitrates decrease with increasing temperature, and that in contrast the peak intensities of acetates (1454 and 1592 cm^{-1}) and formates (1377 cm^{-1}) are increased. Hence they concluded that the activation of propylene started from the low temperatures and increased relatively at high temperatures [38]. With the appearance of formate (HCOO) and acetate (CH_3COO) species, isocyanate (Cu–NCO) and Al–NCO (2197 and 2234 cm^{-1}) also appeared [38,39]. Similarly with an increase in temperature the formation of organic nitrito (R-ONO) and nitro (R-NO_2) species are also observed at 1593 and 1669 cm^{-1} bands. This indicates that the formation of isocyanate species is closely related to the formation of oxygenated hydrocarbon species. The increase in intensity of acetate, formate and carbonates with temperature indicates that the nitrates ($NO + O_2$) chemically react with hydrocarbon species to take part in hydrocarbon oxidation to the carboxylates and carbonates. The bands due to Al–NCO, Cu–NCO and CN also appear by the reaction of nitrates ($NO + O_2$) with C_3H_6 or $C_3H_6 + O_2$, which indicates the N-insertion from the nitrates ($NO + O_2$) to hydrocarbon or partially oxidized (acetates) hydrocarbon species. With increasing temperature, the bands of nitrate decrease promptly, while the Cu–NCO bands gradually increase. The adsorption bands at 3000–2900 cm^{-1} are due to the C–H stretching vibration mode of the adsorbed formate species [40]. In the O–H stretching region of the spectra the bands with negative absorbance appear at above 3770 cm^{-1}. The two bands appeared at 3770 and 3742 cm^{-1}, which may suggest that the adsorption sites of acetate on the catalysts are not associated with Al_{CUS}–O site but associated with the Cu_{CUS}–O site [17]. It is also observed from the DRIFT spectra (Figs. 10(iii) and 11(iii)) that there is no formation of –NH (3223 cm^{-1}) species [39] at high Cu loadings, because of the direct combustion of hydrocarbons. Therefore there is less formation of acetates and hence there is no reaction between NO_2 and acetates for the generation of –NH band. In contrast, with the decrease in Cu loadings, an increase in the intensity of the –NH band is observed

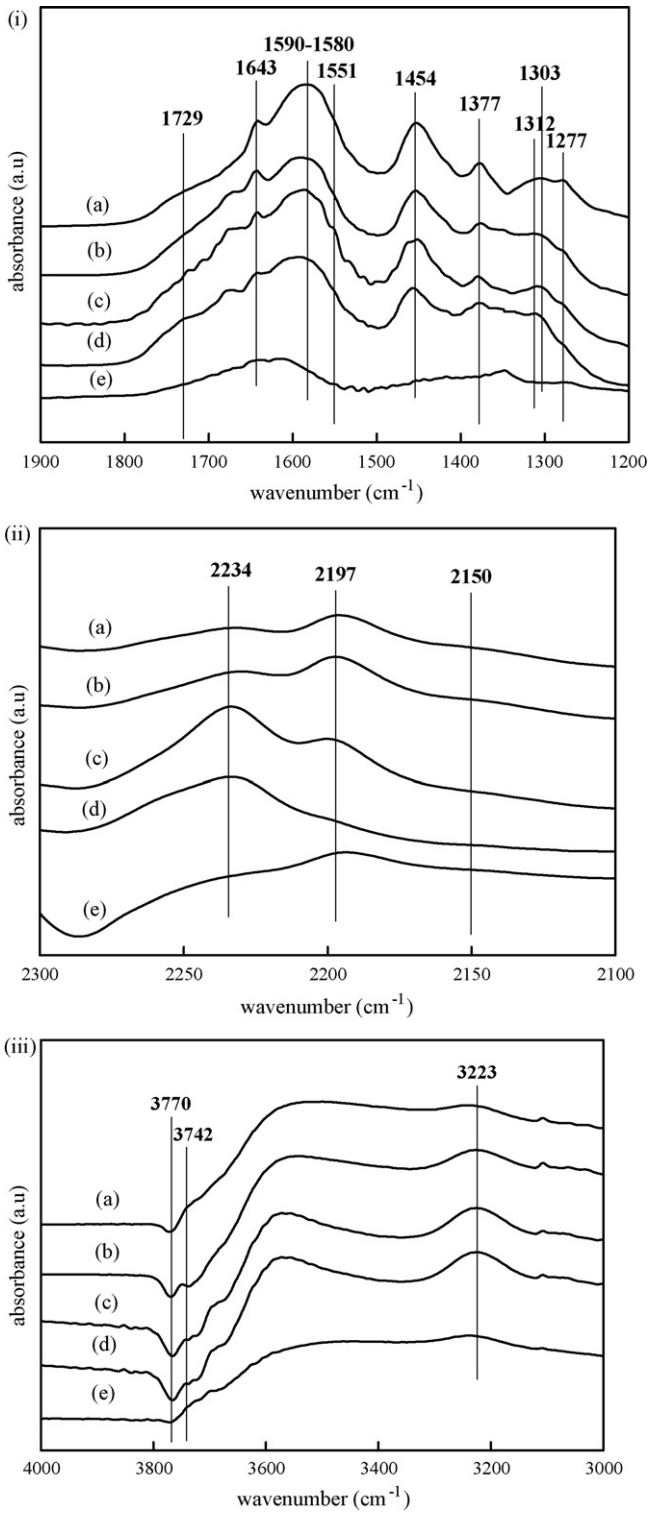

Fig. 10. In situ DRIFT spectra of the catalysts in a steady state at 275 °C in a flow of $NO + C_3H_6 + O_2$. (a) Cu–Al (4:6); (b) Cu–Al (3:7); (c) Cu–Al (2:8); (d) Cu–Al (1:9); (e) Cu–Al (7:3).

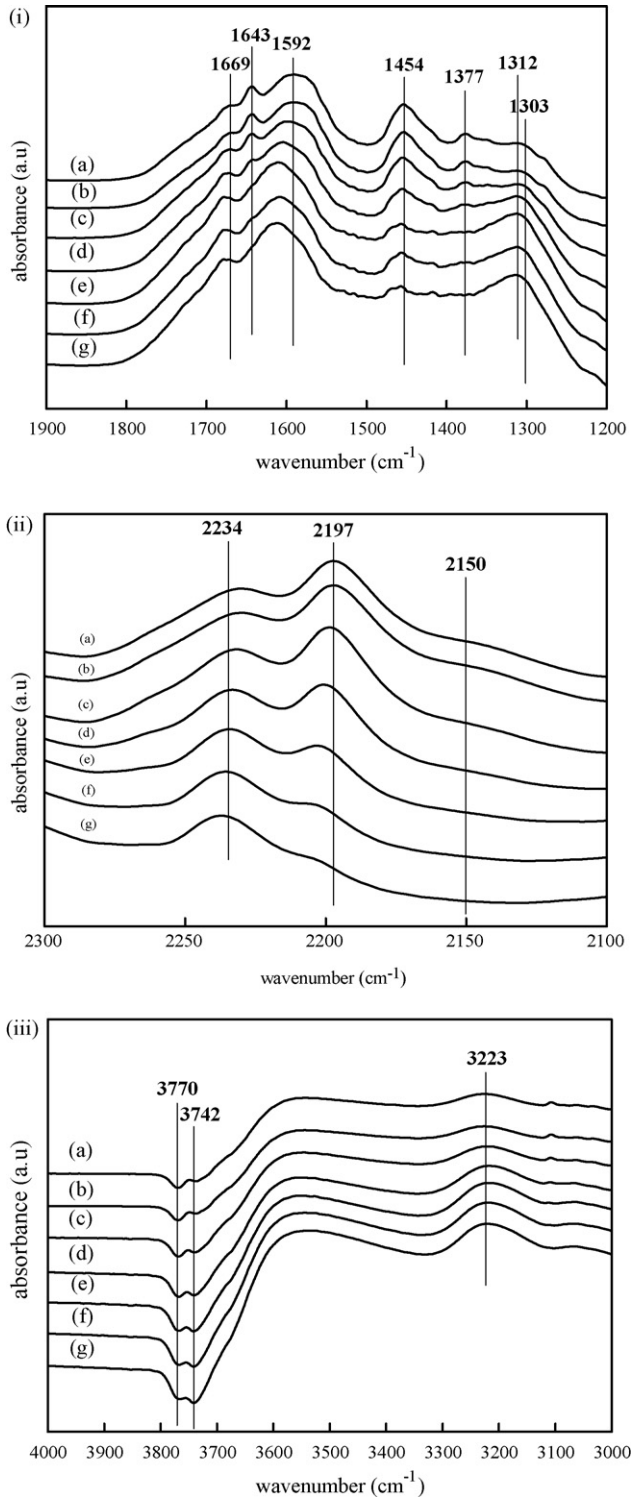

Fig. 11. In situ DRIFT spectra of Cu–Al (3:7) catalyst in a steady state at different temperatures in a flow of NO + C_3H_6 + O_2. (a) 350 °C; (b) 300 °C; (c) 275 °C; (d) 250 °C; (e) 225 °C; (f) 200 °C; (g) 175 °C.

up to Cu–Al (3:7) and it decreases with a decrease in the Cu content, which will form surface complexes with amido groups (–NH complexes). This is assumed by the observation of simultaneous decrease in the –NCO band (2197 cm^{-1}). In conclusion this suggests that the –NCO species are hydrolyzed with –NH complexes by the reaction with some traces of hydroxides present in the catalyst. The hydrolyzed products formed further react with adsorbed NO to be finally converted to N_2 and H_2O.

4. Conclusions

The method of co-precipitation using Na_2CO_3 and NaOH as precipitating agents leads to the formation of LDH (layered double hydroxides) structure. During calcination at high temperatures, highly dispersed CuO and $CuAl_2O_4$ species are produced. The presence of highly dispersed Cu^{2+} phases is confirmed by the XPS and TPR. The TPR analysis revealed a single reduction peak of Cu^{2+}. The order of NO to N_2 conversion is as follows Cu–Al (3:7) > Cu–Al (2:8) > Cu–Al (4:6) > Cu–Al (1:9) > Cu (7:3). The highest NO conversion to N_2 was obtained over the Cu–Al (3:7) catalyst at 300 °C. The peak centered at a binding energy of 935.2 eV is assigned to the Cu^{2+} phase in the form of $CuAl_2O_4$. The formation of LDH structure and highly dispersed Cu^{2+} phase in the form of copper oxide (CuO) and copper aluminate ($CuAl_2O_4$) phases are the key to obtaining high efficiency (70%) in a wide range (250–400 °C) of temperatures. In situ DRIFT spectroscopy studies well confirmed the analysis of timely evolution of different intermediate species, and concluded that the loading of Cu influences the efficient conversion of NO to N_2. Overall it is concluded that the low temperature conversion of NO to N_2 over the Cu–Al (3:7) catalyst is probably due to high surface availability of copper (% intensity of 44.8), particularly as $CuAl_2O_4$ phase with a high percent intensity of 44.

Acknowledgements

This research work was supported by a grant (07K1501-01812) from 'Center for Nanostructured Materials Technology' under '21st Century Frontier R&D Programs' of the Ministry of Science and Technology, Korea.

References

[1] A.C. Stern, R.W. Boubel, D.B. Turner, D.L. Fox, in: D.L. Fox (Ed.), Fundamentals of Air Pollution, Academic Press, New York, 1984, p. 1.
[2] V.I. PaÃrvulescu, P. Grange, B. Delmon, Catal. Today 46 (1998) 233–316.
[3] R. Burch, J.P. Breen, F.C. Meunier, Appl. Catal. B 39 (2002) 283–303.
[4] M. Wojciechowska, S. Lomnicki, Clean Prod. Proc. 1 (1999) 237–247.
[5] K.A. Bethke, M.C. Kung, B. Yang, M. Shah, D. Alt, C. Li, H.H. Kung, Catal. Today 26 (1995) 169–183.
[6] Y. Nagai, T. Yamamoto, T. Tanaka, S. Yoshida, T. Nonaka, T. Okamoto, A. Suda, M. Sugiura, Catal. Today 74 (2002) 225–234.
[7] K. Masuda, K. Tsujimura, K. Shinoda, T. Kato, Appl. Catal. B 8 (1996) 33–40.
[8] T. Zhu, J. Hao, W. Li, Chem. Lett. (2000) 478–481.
[9] H. He, Y. Yu, Catal. Today 100 (2005) 37–47.
[10] F. Severino, J.L. Brito, J. Laine, J.L.G. Fierro, A.L. Agudoy, J. Catal. 177 (1998) 82–95.
[11] H. Hamada, Catal. Today 22 (1994) 21–40.
[12] A. Dandekar, M.A. Vannice, Appl. Catal. B 22 (1999) 179–200.
[13] B.J. Adelman, T. Beutel, G.-D. Lei, W.M.H. Sachtler, J. Catal. 158 (1996) 327–335.
[14] D.B. Lukyanov, E.A. Lombardo, G.A. Sill, J.L. d'Itri, W.K. Hall, J. Catal. 163 (1996) 447–456.
[15] F.C. Meunier, J.P. Breen, V. Zuzaniuk, M. Olsson, J.R.H. Ross, J. Catal. 187 (1999) 493–505.
[16] K. Shimizu, H. Maeshima, H. Yoshida, A. Satsuma, T. Hattori, Phys. Chem. Chem. Phys. 2 (2000) 2435–2439.
[17] K. Shimizu, H. Kawabata, H. Maeshima, A. Satsuma, T. Hattori, J. Phys. Chem. B 104 (2000) 2885–2893.
[18] H. Praliaud, S. Mikhailenko, Z. Chajar, M. Primet, Appl. Catal. B 16 (1998) 359–374.
[19] A. Alejandre, F. Medina, X. Rodriguez, P. Salagre, J.E. Sueiras, J. Catal. 188 (1999) 311–324.
[20] A. Corma, A.E. Palomares, F. Rey, F. Márquez, J. Catal. 170 (1997) 140–149.
[21] S.R. Segal, K.B. Anderson, K.A. Carrado, C.L. Marshall, Appl. Catal. A 231 (2003) 215–226.
[22] A.J. Marchi, D.A. Gordo, A.F. Trasarti, C.R. Apesteguía, Appl. Catal. A 249 (2003) 53–67.
[23] M. Fernández-García, I. Rodríguez-Ramos, P. Ferreira-Aparicio, A. Guerrero-Ruizy, J. Catal. 178 (1998) 253–263.
[24] L. Zhang, F. Li, D.G. Evans, X. Duan, Mater. Chem. Phys. 87 (2004) 402–410 (and references there in).

[25] W.P. Dow, Y.P. Wang, T.J. Huang, J. Catal. 160 (1996) 155–170.
[26] F. Amano, S. Suzuki, T. Yamamoto, T. Tanaka, Appl. Catal. B 64 (2006) 282–289.
[27] V.K. Kaushik, Ch. Sivaraj, P.K. Rao, Appl. Surf. Sci. 51 (1991) 27–33.
[28] K. Shimizua, H. Maeshimaa, A. Satsumaa, T. Hattori, Appl. Catal. B 18 (1998) 163–170.
[29] B.R. Strohmeier, D.E. Levden, R.S. Field, D.M. Hercules, J. Catal. 94 (1985) 514–530.
[30] S.F. Tikhov, V.A. Sadykov, G.N. Kryukova, E.A. Paukshtis, V.V. Popovskii, T.G. Starostina, G.V. Kharlamov, V.F. Anufrienko, V.F. Poluboyarov, V.A. Razdobarov, N.N. Bulgakov, A.V. Kalinkin, J. Catal. 134 (1992) 506–524.
[31] J. Batista, A. Pintar, D. Mandrino, M. Jenko, V. Martin, Appl. Catal. A 206 (2001) 113–124.
[32] T.W. Kim, M.W. Song, H.L. Koh, K.L. Kim, Appl. Catal. A 210 (2001) 35–44.
[33] L. Chen, T. Horiuchi, T. Osaki, T. Mori, Appl. Catal. B 23 (1999) 259–269.
[34] K. Shimizu, J. Shibata, H. Yoshida, A. Satsuma, T. Hattori, Appl. Catal. B 30 (2001) 151–162.
[35] Y. Yu, H. He, Q. Feng, H. Gao, X. Yang, Appl. Catal. B 49 (2004) 159–171.
[36] K. Eränen, F. Klingstedt, K. Arve, L.E. Lindfors, D.Y. Murzin, J. Catal. 227 (2004) 328–343.
[37] C. He, M. Paulus, J. Find, J.A. Nickl, H.J. Eberle, J. Spengler, W. Chu, K. Köhler, J. Phys. Chem. B 109 (2005) 15906–15914.
[38] K. Sato, T. Yoshinari, Y. Kintaichi, M. Haneda, H. Hamada, Appl. Catal. B 44 (2003) 67–78.
[39] M. Haneda, N. Bion, M. Daturi, J. Saussey, J.C. Lavalley, D. Duprez, H. Hamada, J. Catal. 206 (2002) 114–124.
[40] M. Haneda, Y. Kintaichi, N. Bion, H. Hamada, Appl. Catal. B 42 (2003) 57–68.